PIER Letters

(Received 18 August 2024, Accepted 12 September 2024, Scheduled 19 September 2024)

Miniaturized Filter Unit Based on Serpentine Microstrip Resonator and Half-Mode Substrate Integrated Waveguide and Its Application

Lianxin Li, Xiaohei Yan*, Fupeng Wei, Guiqing Liao, Weijun Yu, and Keyou He

School of Physics and Electronic Information Engineering, Guangxi Minzu Normal University, Chongzuo 532200, China

ABSTRACT: In order to effectively reduce the loss of the filter, decrease its size, and improve its frequency selectivity, a miniature filter unit has been proposed. This unit offers enhanced frequency selectivity and facilitates adjustment of the center frequency. The filter unit is constructed by embedding a serpentine microstrip resonator in the upper metallic surface of a half-mode substrate-integrated waveguide (HMSIW). The center frequency of the filter unit is considerably lower than the cutoff frequency of the HMSIW, which contributes to the miniaturization of the filter. The center frequency of the filter unit can be adjusted solely by modifying the dimensions of the microstrip resonator, while the dimensions of the remaining components can be maintained at a constant value. A transmission zero has been incorporated into the upper resistance band with the objective of enhancing its frequency selectivity. A second-order filter with a center frequency of 3 GHz is accurately designed using this filter unit. The results demonstrate that a miniaturized filter with the desired center frequency and excellent performance can be rapidly achieved using this filter unit, which has potential applications in the 5G (sub-6G) band.

1. INTRODUCTION

With the rapid advancement of wireless communication, filters have emerged as crucial frequency selection devices with immense potential for application. In a typical wireless transceiver system, filters play a pivotal role in each link by effectively eliminating noise and ensuring the stability of the RF system. Consequently, they exert a significant influence on the transmission quality of wireless communication systems. To cater to the demands of modern wireless communication, extensive research has been conducted by scholars focusing on enhancing out-of-band rejection, minimizing insertion loss, and achieving miniaturization.

In recent years, substrate-integrated waveguides (SIWs) have gained significant popularity in filter design due to their inherent advantages such as high-quality factor, cost-effectiveness, low loss, and convenient planar integration [1–6]. However, compared to other types of filters, SIW filters present challenges in terms of size. Therefore, various techniques have been proposed to miniaturize SIW filters. Common methods for reducing the size of SIW filters include 1/n mode cutting method, multi-layer folding method, and surface loading method [7–14].

In a previous study, a miniaturized filter was created by metal-etching a complementary split-ring resonator ring (CSRR) in the upper surface of the SIW [7]. However, that filter had a large insertion loss and inconvenient frequency tuning. Another study reduced the filter size by using a multilayer quarter-mode substrate-integrated waveguide (QMSIW) structure and a miniaturized multilayer dual-mode microstrip resonator [8]. However, the filter structure was relatively complex, and the frequency tuning was not convenient. Ref. [9] proposed a miniaturized band-pass filter that utilized a half-mode substrate integrated waveguide (HMSIW) and an embedded e-type defected ground structure (DGS). The filter had a wide bandwidth, but its miniaturization and frequency tuning were complex. Ref. [10] proposed a compact bandpass filter for substrate-integrated waveguides (SIWs) that incorporated a novel diamond-shaped CSRR. The filter included a transmission zero, but its size was relatively large. Ref. [11] proposed an improved QMSIW technique to design a miniaturized filter with a better-quality factor. However, the special shape of the filter limited its application. Ref. [12] introduced a novel miniaturized band-pass filter (BPF) that utilized a hybrid structure. The filter employed shielded QMSIW and microstrip technology, providing a wide passband and high rejection band. However, further improvements were necessary to enhance its miniaturization. Ref. [13] proposed a highly miniaturized dual-mode BPF that used a QMSIW. The filter was realized by etching three slot lines on the upper metal surface of the QMSIW. Although the filter had the advantages of a wide passband and miniaturization, it had poor selectivity on both sides of the passband. In [14], a simple method was presented to realize a miniaturized dual band-pass filter using e-shaped slot lines. The filter offered the advantage of flexible control over the center frequency, but it had a high insertion loss.

* Corresponding author: Xiaohei Yan (yanxiaohei@gxnun.edu.cn).

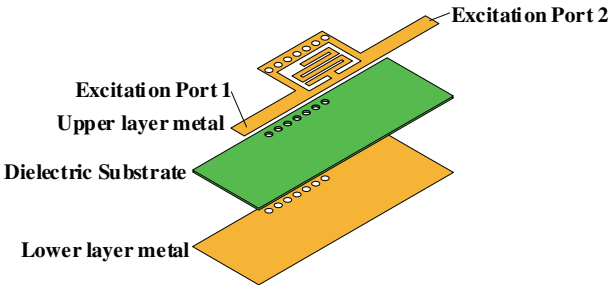

FIGURE 1. Structure of the filter unit.

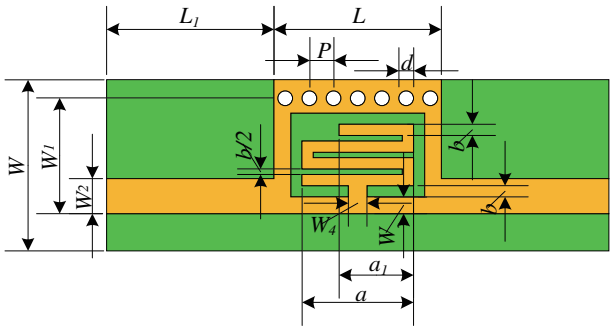

FIGURE 2. Dimensional drawing of the upper metal surface of the filter unit.

The filters proposed in the literature have not achieved a comprehensive balance among several aspects, such as low insertion loss, miniaturization, and easy adjustment of the center frequency. Based on the electric dipole-loaded evanescent-mode theory [15], a serpentine microstrip resonator is embedded in the upper metal surface of a half-mode substrate integrated waveguide (HMSIW) to create a miniaturized filter unit. This approach allows for a smaller filter size and easy center frequency adjustment. Using this filter unit, a second-order filter with the desired center frequency is accurately designed. The filter is then processed and measured to verify the validity of the design. This study aims to reduce the complexity of the filter structure and provide a filter design with low insertion loss, miniaturization, and an easily adjustable center frequency.

2. FILTER UNIT DESIGN

2.1. Structure of the Filter Unit

The filter unit utilizes an HMSIW with a single layer. Figure 1 displays a three-dimensional structure of the filter unit, which comprises two metal layers and one dielectric layer. The dielectric layer is composed of ZYF300CA-P, which has a relative permittivity of 3, a loss tangent of 0.0018, and a thickness of 0.762 mm. The structure contains a serpentine microstrip resonator embedded in the upper metal surface of a HMSIW. The filter unit uses a 50-ohm microstrip line for both input and output ports. Figure 2 shows the upper metal surface with its dimensions. The center frequency of the filter unit is adjustable, with dimension a for coarse adjustment and dimension a_1 for fine adjustment. Table 1 lists the other dimensions of the filter unit.

TABLE 1. Structural parameters of the filter unit (unit: mm).

$L = 9$	$P = 1.3$	$d = 0.8$	$W = 9.2$
$W_1 = 6.2$	$W_2 = 1.88$	$L_1 = 5$	$b = 0.6$
$W_3 = 0.9$	$W_4 = 1$		

2.2. Operating Principle of the Filter Unit

The half-mode substrate integrated waveguide (HMSIW) is obtained by cutting the SIW along its longitudinal centerline, resulting in a transverse dimension that is approximately half that of the SIW. The main mode electric field distribution of the HMSIW is also about half that of the SIW, as the plane where the narrow wall of the HMSIW is located can be equated to a magnetic wall, as shown in Figure 3.

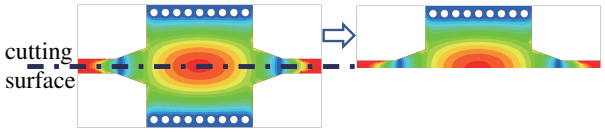

FIGURE 3. Electric field plots in SIW and HMSIW.

The conduction inside the HMSIW is in the $TE_{m+0.5,0}$ mode (where m takes values of 0, 1, 2, 3, etc.) When m equals 0, it corresponds to the main mode of the HMSIW (quasi $TE_{0.5,0}$ mode). The cutoff frequency of this mode can be calculated using the following equation:

$$f_c = \frac{c_0}{4W_{\textit{eff-HMSIW}}\sqrt{\varepsilon_r}} \tag{1}$$

where c_0 is the speed of light in vacuum, ε_r the dielectric constant of the dielectric substrate, and $W_{\textit{eff-HMSIW}}$ the equivalent width of the HMSIW. $W_{\textit{eff-HMSIW}}$ is calculated as:

$$W_{\textit{eff-HMSIW}} = \frac{W_{\textit{eff-SIW}}}{2} + \Delta w \tag{2}$$

where $W_{\textit{eff-SIW}}$ is the equivalent width of the SIW, and Δw is the additional width introduced by the edge effect on the open side. $W_{\textit{eff-SIW}}$ can be calculated by the following equation:

$$W_{\textit{eff-SIW}} = W_{SIW} - \frac{d^2}{0.95P} \tag{3}$$

W_{SIW} is defined as the distance between two rows of circular holes on the broad side of the SIW. The diameter of the circular holes is represented by d, and P represents the distance between adjacent circular holes.

Determining Δw is a complex process that depends on the dielectric substrate's relative permittivity (ε_r), thickness (h), and the equivalent width of the SIW ($W_{\textit{eff-SIW}}$). A highly accurate equation was derived through extensive numerical fitting in [16]:

$$\frac{\Delta w}{h} = \left(0.05 + \frac{0.3}{\varepsilon_r}\right) \cdot \ln\left(\frac{0.79(W_{\textit{eff-SIW}}/2)^2}{h^3}\right.$$

$$+\frac{104(W_{eff\text{-}SIW}/2)-261}{h^2}+\frac{38}{h}+2.77\Bigg) \quad (4)$$

In Table 1, the dimensions show that $W_{SIW} = 2W_1 = 12.4\,\text{mm}$. Without embedding the serpentine microstrip resonator in the HMSIW, the cutoff frequency of the HMSIW can be calculated from the above equation:

$$f_c = 7.15\,\text{GHz} \quad (5)$$

HMSIW can be used as a high-pass filter due to its high-pass characteristics. To create a band-pass filter using HMSIW, an electromagnetic structure with band-stop characteristics must be incorporated into the HMSIW structure. According to the evanescent-mode theory of electric dipole loading [14], the gap structure of the complementary split-ring resonator ring (CSRR) can be etched onto the metal surface of the HMSIW. This design introduces a structure with negative permeability characteristics, which generates strong out-of-band rejection around the resonance frequency. This results in the creation of transmission zeros and a passband for the filter. The proposed design includes a filter unit with a serpentine microstrip resonator embedded in the upper metal surface of the HMSIW. This structure is similar to the CSRR etched in the metal surface of the HMSIW, allowing for the realization of a band-pass filter. Embedding the resonator modifies the internal electric field of the HMSIW, creating a passband below its cutoff frequency. The microstrip resonator utilized in this design is serpentine, which increases the etching slot compared to the general CSRR, resulting in a greater number of surface current paths and a lower passband than the cutoff frequency of the HMSIW. This enables better filter miniaturization. The serpentine microstrip resonator can be conceptualized as a shorted 1/4 wavelength resonator, and its total length can be initially determined by the following equation.

$$l_R = \frac{c_0}{\sqrt{\varepsilon_e}}\frac{1}{4f_0} \quad (6)$$

where ε_e is the equivalent dielectric constant of the microstrip resonator, and f_0 is the resonant frequency of the resonator.

Figure 4 illustrates a comparison of the S-parameters of the present filter unit with a filter unit comprising a normal CSRR of identical dimensions. It can be observed that the center frequency of the present filter unit is markedly lower, and there is a transmission zero on the right side of the passband, thereby enhancing selectivity.

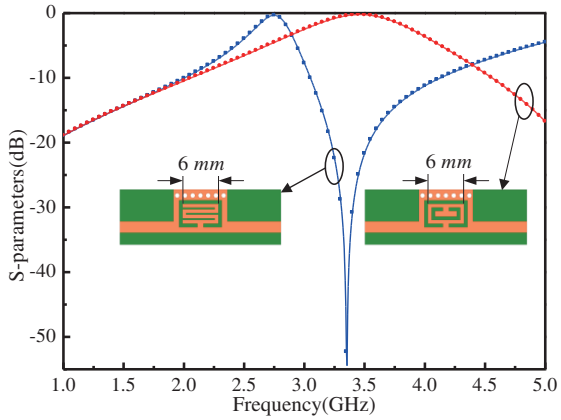

FIGURE 4. Comparison of S-parameters between the present filter unit and the filter unit consisting of a common CSRR.

Figure 5 displays the equivalent circuit model of the filter unit. The row of metal vias on the HMSIW represents a shunt inductor, L_v, which provides the high-pass characteristic. The serpentine microstrip resonator acts as a shunt resonator, equivalent to a capacitor C_r and an inductor L_r, and provides bandpass characteristics. The coupling between the HMSIW and serpentine microstrip resonator is represented by the coupling inductor L_c and coupling capacitor C_c, which provide band-stop characteristics. The equivalent circuit model was simulated using ADS software. The simulation results for $a = a_1 = 6\,\text{mm}$ are displayed in Figure 6, which are consistent with those of HFSS within the designated frequency range, confirming their equivalence.

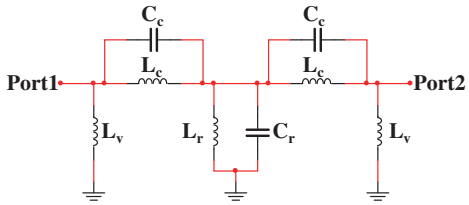

L_v=1.14 nH, L_r =1 nH, C_r=3.4 pF, L_c =1 nH, C_c=2.09 pF

FIGURE 5. Equivalent circuit model of the filter unit.

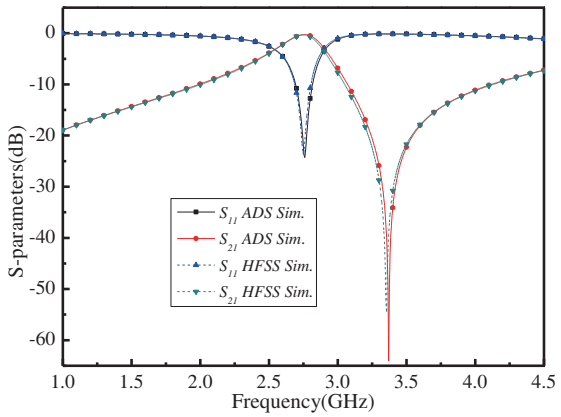

FIGURE 6. ADS simulation results and HFSS simulation results for the filter unit.

2.3. Frequency Adjustment of the Filter Unit

The proposed filter unit in this study allows for easy adjustment of the center frequency by adjusting only dimension a or a_1 while keeping other dimensions constant. A rough center frequency adjustment can be achieved by adjusting dimension a. Figure 7 illustrates the variation of the S-parameter curve of the filter unit with 'a' when $a_1 = a$. Figure 8 shows the curve of the center frequency of the filter unit as 'a' changes. The center frequency of the filter unit changes almost linearly with 'a', and its rate of change can reach 0.56 GHz/mm. The reduction of 'a' slightly broadens the bandwidth of the filter unit, but the return loss remains better than 20 dB.

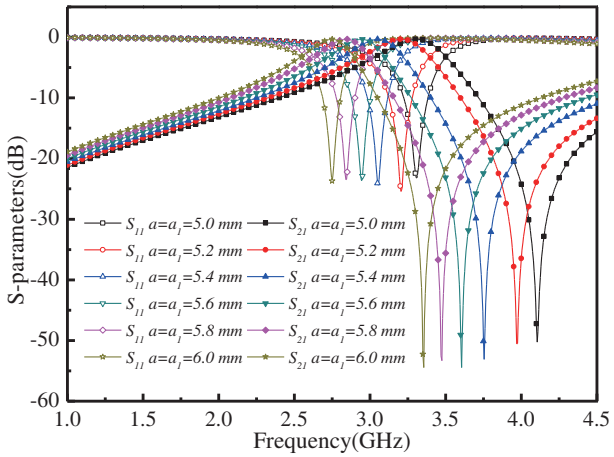

FIGURE 7. The S-parameter curve of the filter unit changes with a.

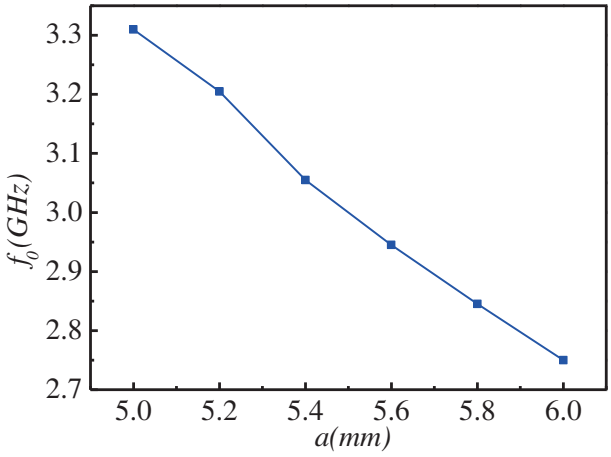

FIGURE 8. The curve of the center frequency of the filter unit as a function of a.

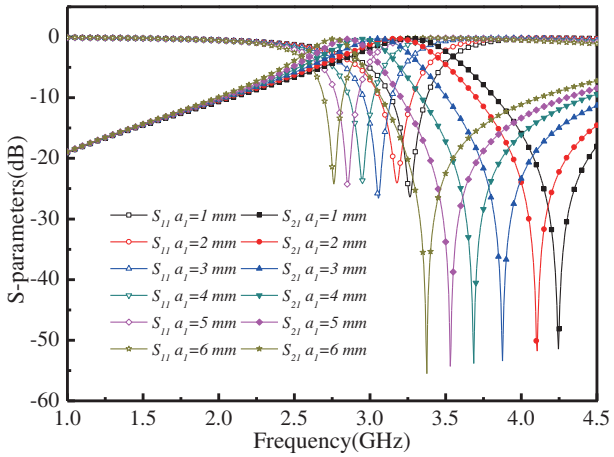

FIGURE 9. The S-parameter curve of the filter unit changes with a_1.

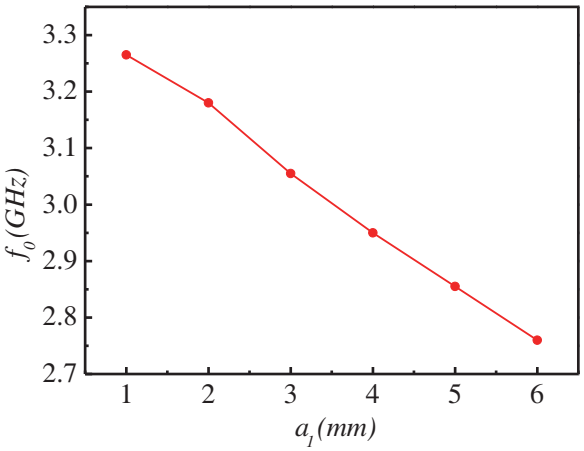

FIGURE 10. The curve of the center frequency of the filter unit as a function of a_1.

When a_1 is not equal to a, the center frequency of the filter unit can be finely tuned by adjusting the size of a_1. The simulation curve of the S-parameter of the filter unit with the change of a_1 when $a = 6$ mm is shown in Figure 9. The curve of the center frequency of the filter unit changing with a_1 is shown in Figure 10. It can be observed that the center frequency of the filter unit changes nearly linearly with a_1, and its rate of change is about 0.1 GHz/mm. During the process of reducing a_1, the filter unit's bandwidth may be broadened to a certain degree, but the return loss will always be better than 20 dB.

3. SECOND-ORDER FILTER DESIGN BASED ON THE FILTER UNIT

3.1. Structure of the Second-Order Filter

The use of the filter unit described above in filter design is demonstrated by accurately designing a second-order filter with a center frequency of 3 GHz. The proposed filter structure is shown in Figure 11, consisting of two symmetrically arranged filter units. Two metal vias are placed between the filter units to control the coupling strength. Figure 12 displays the dimensions of the upper metal surface.

3.2. Determination of Dimension a and Dimension a_1

In general, when two filter units are cascaded, the center frequency of the filter unit shifts towards high frequencies. Based on Figure 8, a dimension of $a = 6$ mm is selected. Next, the dimension of a_1 is adjusted to increase the center frequency of the filter up to 3 GHz. Figure 13 displays the simulation curves of the S-parameters of the second-order filter with the variation of a_1. It is evident that reducing a_1 from 6 mm to 4 mm increases the center frequency of the filter from 2.9 GHz to 3.1 GHz, which is consistent with the filter unit's change rule. When a_1 is equal to 5 mm, the center frequency of the filter is 3 GHz.

3.3. Determination of the Coupling Window Size W_5

The coupling strength between filter units is affected by the size of the coupling window. Simulation curves of the S-parameters of the second-order filter with varying W_5 are shown in Fig-

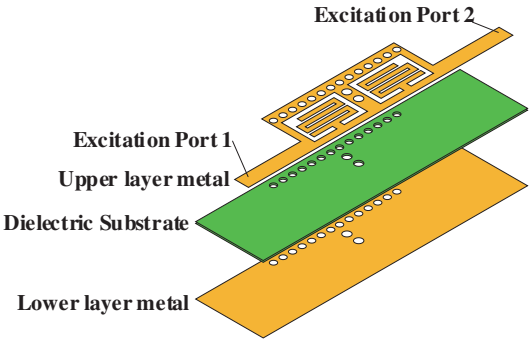

FIGURE 11. Structure of the second-order filter.

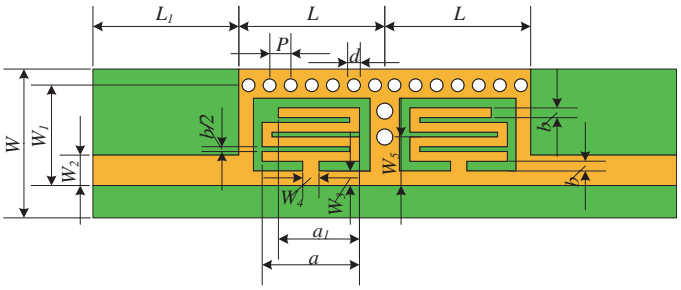

FIGURE 12. Dimensional drawing of the upper metal surface of the second-order filter.

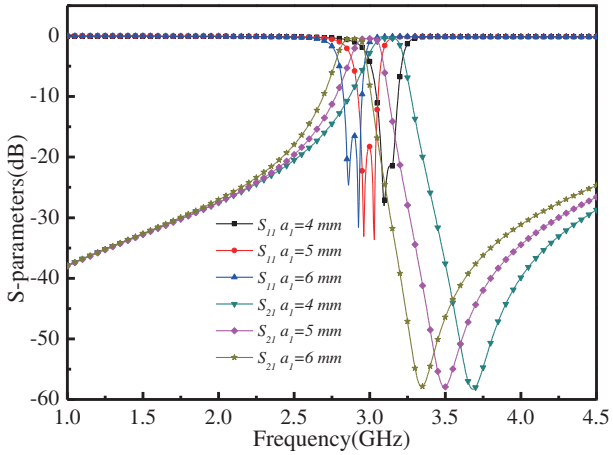

FIGURE 13. The S-parameter curve of the second-order filter varies with a_1.

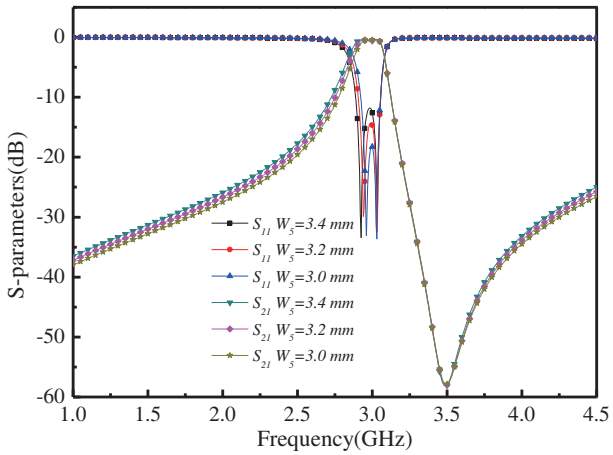

FIGURE 14. The S-parameter curve of the second-order filter varies with W_5.

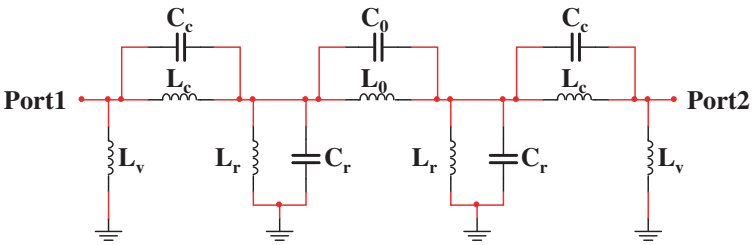

$\mathbf{L_v}$=1.14 nH, $\mathbf{L_r}$=1 nH, $\mathbf{C_r}$=2.81 pF, $\mathbf{L_0}$=10 nH, $\mathbf{C_0}$=24 pF, $\mathbf{L_c}$=1 nH, $\mathbf{C_c}$=2.09 pF

FIGURE 15. Equivalent circuit model of the second-order filter.

ure 14. As W_5 increases, the coupling between the filter units is strengthened, causing a wider bandwidth and greater separation between odd-mode and even-mode frequencies. However, this also results in an increase in return loss. When $W_5 = 3$ mm, the passband of the filter is flatter, and the return loss in the passband is superior. All other dimensional parameters of the second-order filter are the same as the filter unit, and its final dimensional parameters are shown in Table 2.

3.4. Equivalent Circuit Model of the Second-Order Filter

Figure 15 shows the equivalent circuit model of the second-order filter. The model is based on the filter unit with two pairs of new resonators, as two serpentine microstrip resonators are embedded in the upper metal surface of the HMSIW, and there is coupling between them. The shunt resonator introduced by the newly added serpentine microstrip resonator is denoted by L_r and C_r, while the coupling between the two serpentine microstrip resonators is denoted by L_0 and C_0. The equivalent circuit model was simulated using ADS software. The simula-

TABLE 2. Structural parameters of the second-order filter (unit: mm).

$L = 9$	$P = 1.3$	$d = 0.8$	$W = 9.2$	$W_1 = 6.2$
$W_2 = 1.88$	$L_1 = 5$	$b = 0.6$	$W_3 = 0.9$	$W_4 = 1$
$a = 6$	$a_1 = 5$	$W_5 = 3$		

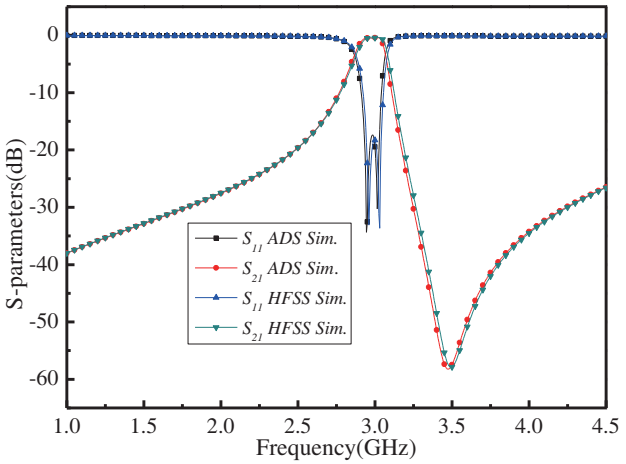

FIGURE 16. ADS simulation results and HFSS simulation results for the second-order filter.

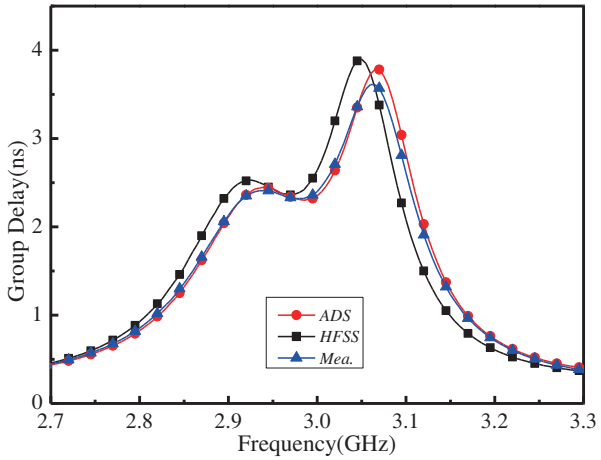

FIGURE 17. The group delay curves of the filter.

TABLE 3. Comparison with similar filters in the literature.

Refs.	F_0 (GHz)	FBW (%)	IL (dB)	RL (dB)	Size (λ_g^2)	Easy adjustment of center frequency
[7]	5.8	10.3%	2.25	11	0.26	×
[8]	8.88	17.6%	1.29	20	0.18	×
[9]	10	23%	1.4	20	0.26	×
[10]	8.86	4.8%	1.2	22	0.34	×
[11]	4	\	1.29	13	0.13	×
[12]	10	22.7%	1.2	14	0.38	×
[13]	1.03	34.8%	0.43	21	0.02	×
[14]	3.6	3.3%	1.3	14	0.17	√
This work	3	6.5%	0.9	18	0.05	√

tion results in Figure 16 are consistent with those obtained from HFSS in the designed frequency band range, which confirms their equivalence. Figure 17 displays the group delay curves of the filter. It is evident that the group delay of the filter is less than 3.9 ns in the passband, and the maximum group delay variation is only 1.4 ns.

3.5. Filter Processing and Testing

To verify the validity of the design results, the designed filter underwent PCB processing. The filter's effective size is 18 mm × 9.2 mm (excluding the input and output ports), and its electrical length is $0.31\lambda_g \times 0.16\lambda_g$, where λ_g is the guided wavelength at the center frequency.

The filter was tested using a vector network analyzer (Agilent E8363C), and the simulation results of the filter S-parameters were compared with the test ones, as shown in Figure 18. The simulation results indicate that the center frequency of the filter is 3 GHz, which is 58% lower than the cutoff frequency of the HMSIW (7.15 GHz). The filter has an insertion loss of 0.4 dB in the passband, a return loss better than 18 dB, and a 3-dB bandwidth of 195 MHz (6.5% relative bandwidth). Additionally, the filter exhibits improved out-of-band rejection performance due to the presence of a transmission zero at 3.5 GHz. The test results indicate that the filter has an insertion loss of only 0.9 dB (0.5 dB greater than the simulated value), a return loss better than 19 dB, and consistent out-of-band rejection performance with the simulation results. The validity of the design is well

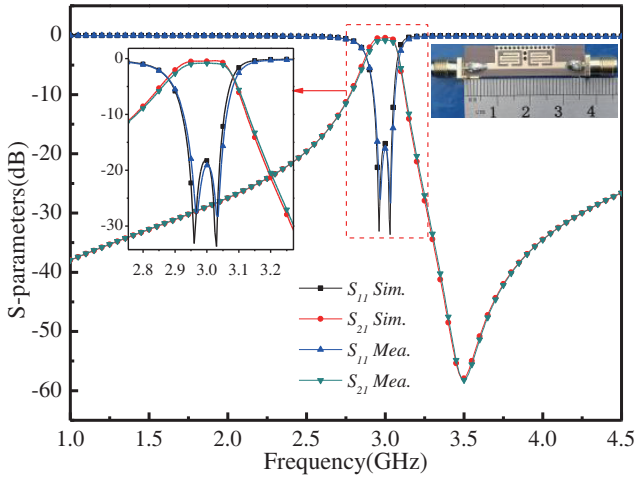

FIGURE 18. Simulation results and test results of the S-parameters of the filter.

verified by the good agreement between the test and simulation results.

Table 3 displays the performance parameters of the second-order filter designed in this paper in comparison to filters proposed in the literature. The results indicate that the filter designed in this paper has advantages in terms of insertion loss, size, and ease of center frequency adjustment.

4. CONCLUSION

A miniaturized filter unit is achieved by embedding a serpentine microstrip resonator in the upper metal surface of a half-mode substrate-integrated waveguide (HMSIW). The center frequency of the filter unit is considerably lower than the cutoff frequency of the HMSIW, which facilitates the miniaturization of the filter. The center frequency of the filter unit can be modified solely by modifying the dimensions of the microstrip resonator, while the remaining dimensions remain unaltered. A transmission zero has been incorporated into the upper resistance band with the objective of enhancing its frequency selectivity. A second-order filter with a center frequency of 3 GHz is accurately designed using this filter unit. The results demonstrate that a miniaturized filter with the desired center frequency and excellent performance can be rapidly achieved using this filter unit, which has potential applications in the 5G (sub-6G) band.

ACKNOWLEDGEMENT

This work is supported by the Guangxi University Student Innovation and Entrepreneurship Training Program Project (No. 202410604020).

REFERENCES

[1] Bozzi, M., A. Georgiadis, and K. Wu, "Review of substrate-integrated waveguide circuits and antennas," *IET Microwaves, Antennas & Propagation*, Vol. 5, No. 8, 909–920, 2011.

[2] Chen, X.-P. and K. Wu, "Substrate integrated waveguide filter: Basic design rules and fundamental structure features," *IEEE Microwave Magazine*, Vol. 15, No. 5, 108–116, 2014.

[3] Zhang, Y.-C., J.-Q. Ge, and G.-A. Wang, "Enabling electrically tunable radio frequency components with advanced microfabrication and thin film techniques," *Journal of Central South University*, Vol. 29, No. 10, 3248–3260, 2022.

[4] Huang, Y. M., W. Jiang, H. Jin, Y. Zhou, S. Leng, G. Wang, and K. Wu, "Substrate-integrated waveguide power combiner/divider incorporating absorbing material," *IEEE Microwave and Wireless Components Letters*, Vol. 27, No. 10, 885–887, 2017.

[5] Jiang, W., W. Shen, T. Wang, Y. M. Huang, Y. Peng, and G. Wang, "Compact dual-band filter using open/short stub loaded stepped impedance resonators (OSLSIRs/SSLSIRs)," *IEEE Microwave and Wireless Components Letters*, Vol. 26, No. 9, 672–674, 2016.

[6] Yan, X. and M. Guo, "Realization of a wide stopband filter using the weakest electric field method and electromagnetic hybrid coupling method," *International Journal of RF and Microwave Computer-Aided Engineering*, Vol. 2024, No. 1, 9298815, 2024.

[7] Pu, J., F. Xu, and Y. Li, "Miniaturized substrate integrated waveguide bandpass filters based on novel complementary split ring resonators," in *2019 IEEE MTT-S International Microwave Biomedical Conference (IMBioC)*, Vol. 1, 1–3, Nanjing, China, 2019.

[8] Lin, G., Y. Dong, and X. Luo, "Miniaturized quarter-mode SIW filters loaded by dual-mode microstrip resonator with high selectivity and flexible response," *IEEE Microwave and Wireless Components Letters*, Vol. 32, No. 6, 660–663, Jun. 2022.

[9] Wang, C., Z. Wang, and Y. M. Huang, "Size-miniaturized half-mode substrate integrated waveguide bandpass filter incorporating E-shaped defected ground structure for wideband communication and radar applications," in *2018 20th International Conference on Advanced Communication Technology (ICACT)*, 12–16, Chuncheon, Korea (South), 2018.

[10] Muchhal, N. and S. Srivastava, "Design of miniaturized diamond shaped substrate integrated waveguide CSRR band pass filter for X band applications," in *2019 International Conference on Signal Processing and Communication (ICSC)*, 113–116, Noida, India, 2019.

[11] Delmonte, N., M. Bozzi, L. Perregrini, and C. Tomassoni, "Miniaturized SIW filters based on shielded quarter-mode cavities," in *2019 IEEE MTT-S International Conference on Numerical Electromagnetic and Multiphysics Modeling and Optimization (NEMO)*, 1–3, Boston, MA, USA, 2019.

[12] Zheng, Y., Y. Zhu, Z. Wang, and Y. Dong, "Compact, wide stopband, shielded hybrid filter based on quarter-mode substrate integrated waveguide and microstrip line resonators," *IEEE Microwave and Wireless Components Letters*, Vol. 31, No. 3, 245–248, Mar. 2021.

[13] Barik, R. K., S. Koziel, and S. Szczepanski, "Highly-miniaturized dual-mode bandpass filter based on quarter-mode substrate integrated waveguide with wide stopband," *IEEE Access*, Vol. 10, 42 163–42 170, 2022.

[14] Zhang, H., W. Kang, and W. Wu, "Miniaturized dual-band SIW filters using E-shaped slotlines with controllable center frequencies," *IEEE Microwave and Wireless Components Letters*, Vol. 28, No. 4, 311–313, Apr. 2018.

[15] Danaeian, M., A.-R. Moznebi, and K. Afrooz, "Super compact dual-band substrate integrated waveguide filters and filtering power dividers based on evanescent-mode technique," *AEU — International Journal of Electronics and Communications*, Vol. 125, 153348, 2020.

[16] Lai, Q., C. Fumeaux, W. Hong, and R. Vahldieck, "Characterization of the propagation properties of the half-mode substrate integrated waveguide," *IEEE Transactions on Microwave Theory and Techniques*, Vol. 57, No. 8, 1996–2004, Aug. 2009.